PERFORMANCE STUDY ON A PRINTED CIRCUIT HEAT EXCHANGER COMPOSED OF NOVEL AIRFOIL FINS FOR SUPERCRITICAL CO_2 CYCLE COOLING SYSTEM

by

Yulong MA [a,b*], ***Qingdong HOU*** [a,b], ***and Tianyi WANG*** [a,b]

[a] School of Energy and Power Engineering,
Nanjing University of Aeronautics and Astronautics, Nanjing, China
[b] Key Laboratory of Thermal Management and Energy Utilization of Aviation Vehicles,
Ministry of Industry and Information Technology, Nanjing, China

Original scientific paper
https://doi.org/10.2298/TSCI220408112M

The printed circuit heat exchanger (PCHE) plays a vital role in the supercritical CO_2 cooling system for hypersonic aircraft, which significantly affects the efficiency and stability of the cooling system. In this study, a novel structure is proposed to improve the overall performance of airfoil fin PCHE. The RP-3 aviation kerosene and SCO_2 are used as working fluids to study the thermal-hydraulic performance and the enhancement mechanism. The results indicate that the overall performance of the PCHE can be improved by slotting the airfoil fin. With the increase in groove thickness, the thermal performance of the new airfoil fin PCHE first improves and then worsens, while the hydraulic performance of the PCHE first worsens and then improves. Compared with the original airfoil fin, the fin with a groove thickness of 0.6 mm reduces the pressure drop by up to 15% without affecting the thermal performance, while the fin with a groove thickness of 0.1 mm increases the heat transfer by 4%-5%. In addition, the optimal mass-flow ratio of SCO_2 to kerosene is obtained by thermal resistance matching under different working conditions, which is helpful for the design and optimization of airfoil fin PCHE based on the SCO_2 cycle cooling system for scramjets.

Key words: *printed circuit heat exchanger, supercritical CO_2 cycle, airfoil fin, heat transfer performance, pressure drop*

Introduction

Hydrocarbon fuel regenerative cooling systems are considered an effective thermal protection method for scramjet engines [1]. Hydrocarbon fuel acts as a coolant and absorbs the heat emitted by the engine before entering the combustion chamber. This approach not only cools the engine but also improves the thermal efficiency of the scramjet [2]. Higher flight speed is the main direction for the future development of hypersonic aircraft, which leads to more severe heat load [3]. Endothermic hydrocarbon fuel has been developed to improve the heat capacity of the regenerative cooling systems [4]. However, the hydrocarbon fuel in the conventional regenerative cooling system is easy to coke at high temperature [5], which makes it challenging to meet the reliability of the regenerative cooling system. Therefore, it is urgent to find a new method to satisfy the cooling requirement of hypersonic aircraft.

* Corresponding author, e-mail: mayulong@nuaa.deu.cn

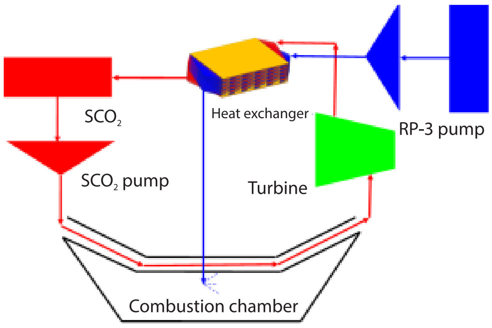

Figure 1. Schematic diagram of SCO_2 cycle cooling system

In recent years, SCO_2 has been proposed as a third fluid to replace hydrocarbon fuel [6]. As depicted in fig. 1, SCO_2 absorbs the heat dissipated from the combustion chamber wall and transfers the heat to the fuel through the heat exchanger. The SCO_2 will not react with the cooling channel of the engine under high temperature conditions due to its high stability, which can ensure the safety of the thermal protection system.

As one of the critical components of the SCO_2 cycle cooling system, the heat exchanger significantly impacts the efficiency and stability of the entire cooling system. The printed circuit heat exchanger is considered one of the most promising candidates for the SCO_2 cycle due to its small size, high efficiency, and good stability. The PCHE is manufactured by diffusion bonding the photochemically etched plates, which ensures the safety and stability of the heat exchanger.

Many scholars have conducted extensive research on various types of PCHE. By comparing the heat transfer and flow of straight channel and zigzag channel PCHE, Meshram *et al.* [7] found that the size of zigzag channel PCHE is much smaller due to their higher heat transfer coefficient. Lee *et al.* [8] investigated the effect of different cross-sectional shapes on the zigzag PCHE, and the results show that the heat transfer performance of the rectangular channel is the best, while that of the circular channel is the worst. Kim *et al.* [9] studied the *f* factor and Nusselt number of a PCHE with various geometric parameters, and they evaluated the performance of the heat exchanger by cost. Lee *et al.* [10] optimized the flow and heat transfer performance of zigzag PCHE by designing the parameters of the channel. They found that the zigzag channel PCHE had the best thermohydraulic performance when the angle of the cold side was similar to that of the hot side.

Compared with the straight channel PCHE, the zigzag channel enhances the heat transfer performance and increases the pressure drop. To solve the problem of excessive pressure drop in the zigzag channel, scholars have proposed novel channels. Ngo *et al.* [11] proposed *S*-shaped fins based on the high pressure drop of the zigzag channel, and they investigated the thermal and flow performance of the new *S*-shaped fin. The results show that compared with the PCHE with the zigzag channel, the PCHE with *S*-shaped fins provides a 6-7 times lower pressure drop under the same heat transfer performance. Lin *et al*. [12] numerically investigated the thermal-hydraulic performance of *Z*-shaped and *S*-shaped channels with various bending angles. The results indicate that the small bending angle is beneficial to the formation of uniform streamlines, and the overall performance of the *S*-shaped channel is better than that of the *Z*-shaped channel. Tsuzuki *et al*. [13] investigated the flow resistance and thermal performance of an *S*-shaped fin PCHE with CO_2, and obtained the best configuration by changing the shape and distribution of the fins.

Some researchers [14] have compared the performance between the zigzag channel PCHE and airfoil fin PCHE under the same working conditions, and they found that the airfoil fin has a smaller pressure drop under the same heat transfer performance. Kwon *et al*. [15] analyzed the *f* factor and Nusselt number with various airfoil fin PCHE. Kim *et al*. [16] explored the performance of PCHE by SCO_2. They found that the arrangement of the fins affects the performance of the PCHE, and they indicated that the airfoil fin PCHE has the best performance when the longitudinal distance between fins is equal to the length of fins. Xu *et al*. [17] studied the effect of fin arrangement on the performance of PCHE and found that staggered airfoil fins have better thermal-hydraulic performance than parallel airfoil fins. An experiment conducted by Ma *et al*. [18] explored the character of the fin-endwall fillet, and they found that the overall performance is improved when the non-dimensional longitudinal pitch is 1.63. Chu *et al*. [19] studied the influence of fin shape on PCHE. They pointed out that a fin with a larger windward area and shorter length has better overall performance. Cui *et al*. [20] optimized the shape of the fin based on the NACA 0020 airfoil fin, and they obtained a new fin with better performance.

As previously shown, the PCHE with an airfoil fin has the best overall performance among the several PCHE, which has enormous potential as a heat exchanger of the SCO_2 cycle cooling system. However, previous studies on the airfoil fin PCHE were mainly to optimize the arrangement of airfoil fins by comparing with the thermal-hydraulic performance of the zigzag channel PCHE. The optimization of the airfoil geometry and thermal resistance matching has seldom been studied. In this paper, a new structure of the airfoil fin is proposed. The enhancement mechanism of the new structure is discussed and analyzed, and the effect of the fin size on the performance of the PCHE is investigated under different working conditions. Meanwhile, the optimal mass-flow ratio of fuel to SCO_2 is obtained by matching the thermal resistance on both sides.

Numerical approach

Physical model and boundary conditions

The simplified model of the original and the new PCHE are shown in fig. 2. The geometry of the original airfoil fin is obtained from NACA 0020, a typical symmetric airfoil fin. The fin height, H_s, fin width, W_s, and fin length, L_s, are set as 0.95 mm, 1.5 mm, and 6 mm, respectively. The values of the longitudinal pitch, L_b, and staggered pitch, L_a, of the original airfoil fin PCHE are fixed as 12 mm and 6 mm, respectively. The values of L_a, L_b, and L_c of the new PCHE are the same as those of the original airfoil fin PCHE. The two simplified airfoil fin PCHE models contain one hot fluid channel and one cold fluid channel, the directions of fins in the two channels are opposite, and the fluid-flows from the head to the tail of the fins. There are ten fins in each plate, and the detailed geometrical parameters of the simulated domain are summarized in tab. 1.

Table 1. Geometrical parameters of the airfoil fin PCHE model

Parameters	Value [mm]	Parameters	Value [mm]
Length of the airfoil fin, L_s	6	Length of the model, L	62.4
Height of the airfoil fin, H_s	0.95	Height of the model, H	3.26
Width of the airfoil fin, W_s	1.2	Width of the model, W	4.8
Staggered pitch, L_a	6	Height of the middle wall, H_w	0.68
Longitudinal pitch, L_b	12	Transverse pitch, L_c	2.4

Figure 2 shows the boundary conditions of the original and new structures of the airfoil fin PCHE. To compare the thermal-hydraulic performance of different fins, the boundary conditions used by different models are the same, and the details are summarized:

– *Inlet boundary condition*, the velocity inlet boundary contains the mass-flow rate and inlet temperature.
– *Outlet boundary condition*, pressure outlet boundary.
– *Top, bottom, left, right walls*, periodic boundary.

– *Interface between the fluid domain and solid domain*, no-slip and coupled boundary.
– *Other walls*, adiabatic boundary.

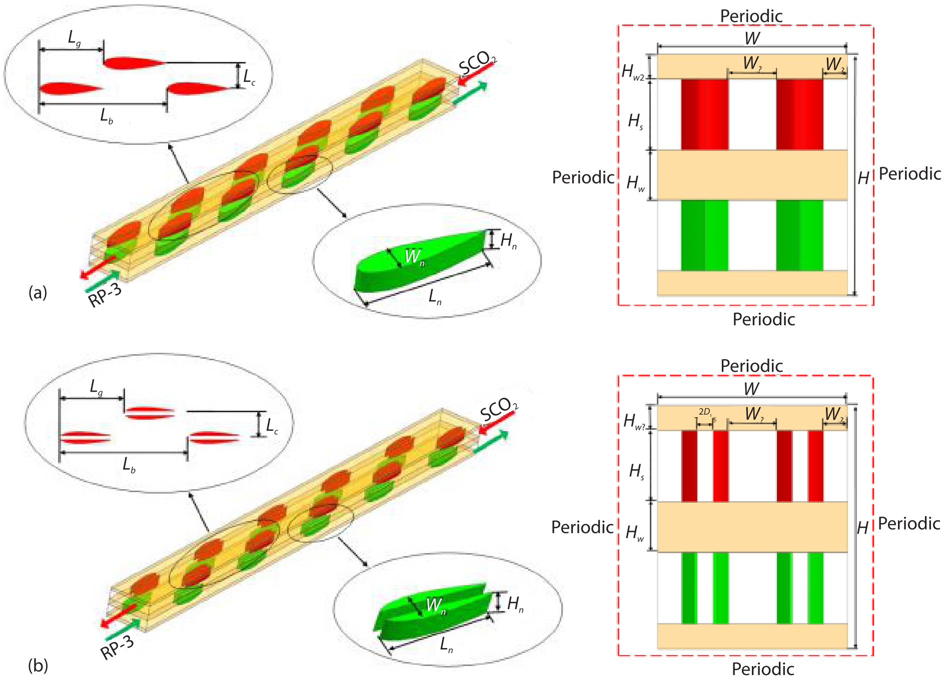

Figure 2. Structure and boundary conditions of the two airfoil fin PCHE model; (a) original airfoil fin PCHE and (b) new airfoil fin PCHE

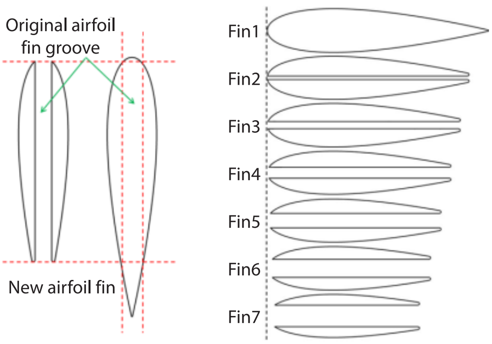

Figure 3. Sketch of original and new airfoil fin

Figure 3 shows that the new structure is obtained by grooving in the center of the original airfoil fin. Fin1 represents the original airfoil fin, whose thickness is 1.2 mm. Seven fins are simulated under the same working conditions to investigate the influence of groove thickness on the flow and heat transfer performance of the PCHE. The main difference between the seven fins is the thickness of the groove, the groove thickness of Fin 1-7 is 0 mm, 0.1 mm, 0.2 mm, 0.3 mm, 0.4 mm, 0.5 mm, and 0.6 mm, respectively.

Governing equations and parameter definitions

Compared with other turbulence models, the SST turbulence model [17, 19] combines the advantages of the k-ε and k-ω models, which is more accurate when simulating the flow and thermal characteristics of SCO_2. The SST turbulence model was chosen as the turbulence model. The FLUENT 19.1 commercial software with double precision is used to solve this issue in this paper. The SIMPLEC algorithm is chosen as the solution method, and the following terms are discretized by second order. The convergence criterion for each equation is set to 10^{-6}. The governing equations are:

$$\frac{\partial}{\partial x_i}(\rho U_i) = 0 \tag{1}$$

$$\frac{\partial}{\partial x_j}\left(\rho u_i u_j\right) = \frac{\partial}{\partial x_j}\left[\left(\mu + \mu_t\right)\left(\frac{\partial u_i}{\partial x_j} + \frac{\partial u_j}{\partial x_i} - \frac{2}{3}\frac{\partial u_k}{\partial x_k}\delta_{ij}\right)\right] - \frac{\partial p}{\partial x_i} \tag{2}$$

$$\frac{\partial}{\partial x_i}\left(\rho u_i h\right) = \frac{\partial}{\partial x_i}\left(\lambda \frac{\partial T}{\partial x_i}\right) + \phi \tag{3}$$

where ϕ is the dissipation function, representing the energy dissipation caused by viscosity.

The Reynolds number is calculated:

$$\mathrm{Re} = \frac{\rho u D_h}{\mu} \tag{4}$$

where ρ, u, μ are the density, velocity, and dynamic viscosity, and D_h is defined:

$$D_h = \frac{4A_h}{P} \tag{5}$$

where A_h is the inlet cross-sectional area and P – the inlet wetted perimeter, and the heat transfer coefficient can be calculated:

$$h = \frac{Q_{\mathrm{ave}}}{A_{\mathrm{RES}}\left(T_{\mathrm{f}} - T_{\mathrm{w}}\right)} \tag{6}$$

where T_{f} is the fluid temperature, T_{w} – the wall temperature, A_{RES} – the representative surface area, and Q_{ave} – the heat transfer rate of PCHE, which is defined:

$$Q_{\mathrm{ave}} = \frac{Q_{\mathrm{hot}} + Q_{\mathrm{cold}}}{2} = \frac{\dot{m}_{\mathrm{hot}}\left(h_{\mathrm{hot,in}} - h_{\mathrm{hot,out}}\right) + \dot{m}_{\mathrm{cold}}\left(h_{\mathrm{cold,in}} - h_{\mathrm{cold,out}}\right)}{2} \tag{7}$$

where h is the enthalpy, the subscript hot and cold rare the hot and cold fluid, in and out – the mean the inlet and outlet of the fluid channel.

A large number of planes are created in the channel along the flow direction due to the changeable thermophysical properties of aviation kerosene and SCO_2. The thermal-hydraulic performance of local planes is calculated. The global parameters are obtained by averaging the data obtained from local sections.

The local Prandtl number and the local Nusselt number can be calculated:

$$\mathrm{Pr}_l = \frac{\mu_l C_{p,l}}{\lambda_l} \tag{8}$$

$$\mathrm{Nu}_l = \frac{h D_h}{\lambda_l} \tag{9}$$

where $C_{p,l}$ is the local specific heat, λ_l – the local heat conductivity, and the local Colburn-*j* factor, j_l, and local Fanning friction factor, f_l, are calculated:

$$j_l = \frac{\mathrm{Nu}_l}{\mathrm{Re}_l \, \mathrm{Pr}_l^{1/3}} \tag{10}$$

$$f_l = \frac{\left(P_{\mathrm{in}} - P_l\right)}{2u_l^2 \rho_l}\frac{D_h}{X_l} \tag{11}$$

The effectiveness of heat transfer, ε, is the ratio of the actual heat transfer rate to the maximum possible heat transfer in the sense of thermodynamics. Therefore, ε has the meaning of heat exchanger efficiency from a thermodynamic point of view. The value of ε reflects the heat transfer performance when the inlet and outlet temperature and mass-flow are fixed. The effectiveness of the heat exchanger is calculated:

$$\varepsilon = \frac{q}{q_{\max}} = \frac{C_{\text{hot}}\left(t_{\text{hot,in}} - t_{\text{hot,out}}\right)}{C_{\min}\left(t_{\text{hot,in}} - t_{\text{cold,in}}\right)} = \frac{C_{\text{cold}}\left(t_{\text{cold.out}} - t_{\text{cold,in}}\right)}{C_{\min}\left(t_{\text{hot},in} - t_{\text{cold,in}}\right)} \tag{12}$$

where C is the heat capacity rate of fluid, $C_{\min}$ – the minimum heat capacity rate between C_{hot} and C_{cold}. The number of heat transfer units (NTU) is a dimensionless measurement of the heat transfer scale of the heat exchanger. A smaller NTU indicates a lower efficiency of the heat exchanger, and a larger NTU indicates a higher efficiency. The NTU is calculated:

$$NTU = \frac{AU}{C_{\min}} \tag{13}$$

where the A is the heat transfer area and U – the overall heat transfer coefficient of the heat exchanger, and U is defined:

$$\frac{1}{UA} = \frac{1}{h_{\text{hot}} A_{\text{hot}}} + \frac{\delta}{\lambda_{\text{w}} A_{\text{w}}} + \frac{1}{h_{\text{cold}} A_{\text{cold}}} \tag{14}$$

In order to compare the overall performance of different PCHE, enhanced ratio η is used to evaluate the comprehensive performance of PCHE in the present work, which is defined:

$$\eta = \frac{\dfrac{j}{j_{\text{Fin1}}}}{\left(\dfrac{f}{f_{\text{Fin1}}}\right)^{1/3}} \tag{15}$$

Mesh generation and model validation

Tetrahedral meshes were used in this work. As shown in fig. 4, the surface and volume mesh of the tail region of the airfoil fin is encrypted. To ensure that y^+ is less than 1, the first layer of the grid is fixed at 0.002 mm, and the increment ratio is 1.2. The grid independence tests were conducted to ensure the accuracy of the simulation results. When the number of nodes is larger than 12216298, the error of the results is relatively small, and it was applied to the simulation models.

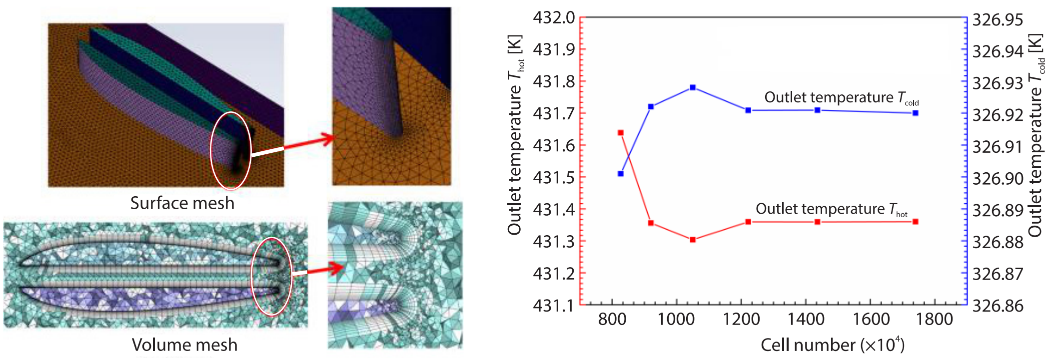

Figure 4. Mesh and grid independent test of the airfoil fin

The simulation results were compared with the results published by Ishizuka *et al.* [21] The simplified model consists of two hot fluid channels and one cold fluid channel. The cold fluid channel is located between the two hot fluid channels, the bending angle is 100°, and the bending angle of the hot fluid channel is 115°. The mass-flow rate of each channel is the same as in the experiment, and the boundary conditions of the top and bottom walls and the left and right walls are set to be periodic. The comparison results are listed in tab. 2. The largest relative error is 8.6%. Taking into account the accuracy of the turbulence model, the measurement accuracy of the experimental instrument, which indicates the calculation results of the work in this paper is reliable and accurate.

Table 2. Comparison with Tsuzuka *et al.* [21] experimental results

	Experimental results	Numerical results	Error [%]
Outlet temperature on cold channel [K]	140.38	136.88	2.5
Outlet temperature on hot channel [K]	169.6	171.461	0.92
Pressure drop on cold channel [Pa]	73220	66909.2	8.6
Pressure drop on hot channel [Pa]	24180	24745.7	2.3

Results and discussion

Thermal and flow analysis along the flow direction

In this section, seven types of PCHE with different airfoil fins are simulated under the same boundary conditions, and aviation kerosene and SCO_2 are taken to study the velocity and pressure field in the fluid channels of different airfoil fins.

The Streamlines of SCO_2 and RP-3 in the fluid channel with Fin1 are shown in fig. 5. The streamlines on both sides of the airfoil fins change periodically due to the periodic arrangement of the airfoil fins. The thickest part of the fin has a minor cross-sectional flow and considerable velocity, and the pressure in this region is relatively low. The fluid collides with

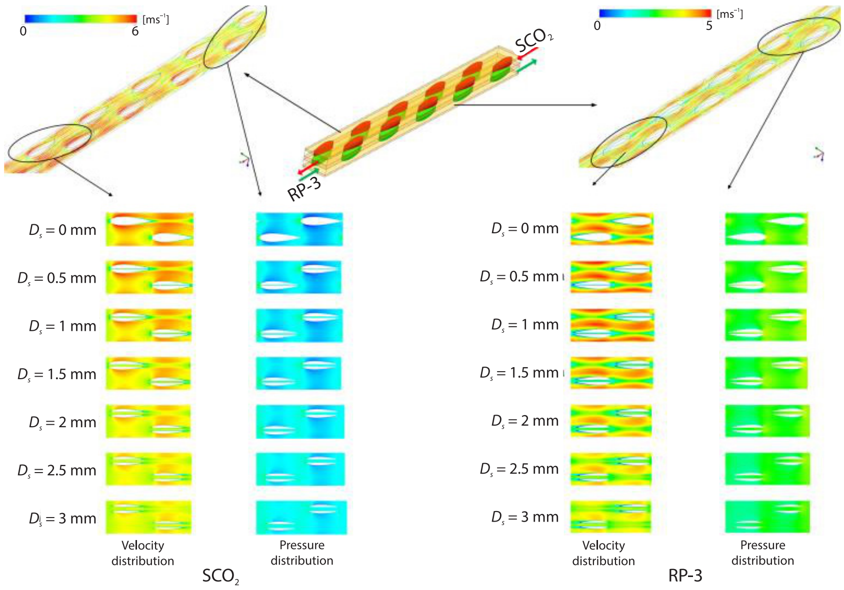

Figure 5. Streamline in the hot and cold fluid channel with different airfoil fins

the fin head, resulting in a relatively low velocity at the head of the fin, and the velocity at the fin tail is also low due to vortex action.

It can be seen from the figure that the velocity of SCO_2 in the hot fluid channel presents a downward trend along the flow direction. This is because as SCO_2 gradually cools, the density of SCO_2 increases with decreasing temperature, resulting in a smaller velocity in the same cross-sectional area. Meanwhile, with the increase in groove thickness, the velocity between the fins in the channel decreases gradually. This is because at the same mass-flow rate, the velocity decreases as the cross-sectional area increases. In contrast to SCO_2, the velocity distribution of aviation kerosene in the cold fluid channel increases along the flow direction. This is because the density of aviation kerosene decreases with increasing temperature. It is worth noting that when the groove thickness is 1 mm, the velocity between fins in the cold channel is larger than that between the original fins. This is because the change in the physical properties of RP-3 has a greater impact on the velocity than the increase in the flow cross-sectional area. At the same time, the distribution of velocity and pressure in the hot and cold channels tends to be steady with increasing groove thickness. This is because the volume of fins decreases with increasing flow cross-sectional area, and the influence of fins on flow becomes weaker.

Comparison of new structure and original airfoil fin PCHE

Figure 6 shows the overall performance of SCO_2 in the hot fluid channel with seven types of fins. The mass-flow rate of SCO_2 is set at 1.6 g/s, 1.2 g/s, 0.8 g/s, and 0.4 g/s, and the mass-flow rate of aviation kerosene is fixed at 9.12 g/s. The inlet temperature of the hot fluid

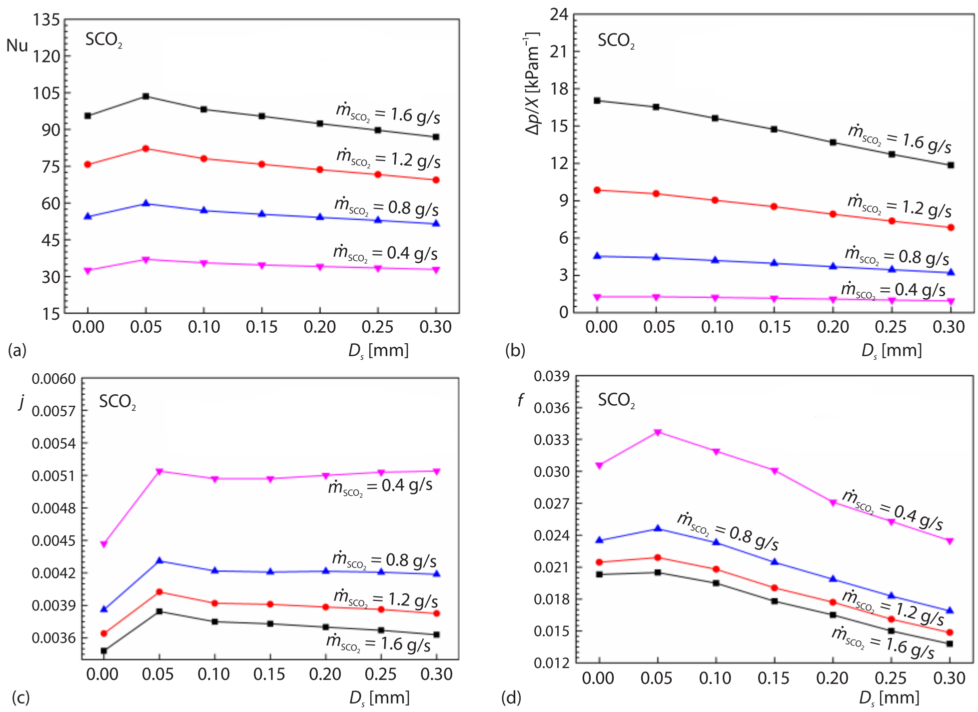

Figure 6. Overall performance of SCO_2 at hot fluid channel with seven types of fins; (a) Nusselt number, (b) pressure drop per flow length, (c) Colburn *j* factor, and (d) Fanning friction factor

channel is set at 500 K and the outlet pressure is set at 8.28 MPa, while the inlet temperature of the cold fluid channel is set at 320 K and the outlet pressure is set at 4 MPa for all simulated cases. Nusselt number increases with increasing mass-flow rate. This can be explained by the more significant mass-flow rate leading to more substantial turbulence in the channel, which improves the heat transfer performance. Figure 6(b) shows that the difference in $\Delta p/X$ between the seven airfoil fins is relatively small under the condition of a low mass-flow rate, and $\Delta p/X$ decreases with increasing groove thickness, which means that grooves in the center of the fins are helpful in reducing the pressure drop. The variations in the Colburn-*j* factor, *j*, and Fanning friction factor, *f*, with various inlet mass-flow rates of different fins are presented in figs. 6(c) and 6(d). Since *j* and *f* are inversely proportional to velocity, *j* and *f* decrease with increasing mass-flow rate. In addition, Fin2 has the most significant *j* factor and *f* factor, indicating that Fin2 has the best heat transfer performance. Meanwhile, the hydraulic performance is the worst because the decrease in pressure drop is smaller than the square of velocity.

Figure 7 shows the flow and heat transfer performance of aviation kerosene in the cold channel. The trend of Nusselt number in fig. 7(a) is similar to that of Nusselt number in the SCO_2 channel because the heat transferred to the fuel increases with the mass-flow in the SCO_2 channel. However, the $\Delta p/X$ shown in fig. 7(b) has different trends with that of $\Delta p/X$ in the SCO_2 channel. First, the pressure drop in the cold channel increases first and then decreases with increasing groove thickness. This is because the change in density in Fin2 increases the flow velocity in the channel, leading to an increase in the pressure drop. With a further increase in groove thickness, the effect of physical property changes on the velocity in the channel is smaller than the effect of the cross-sectional area, and the pressure in the cold channel begins to decrease. Second, the pressure drop in the cold channel decreases with increasing mass-flow

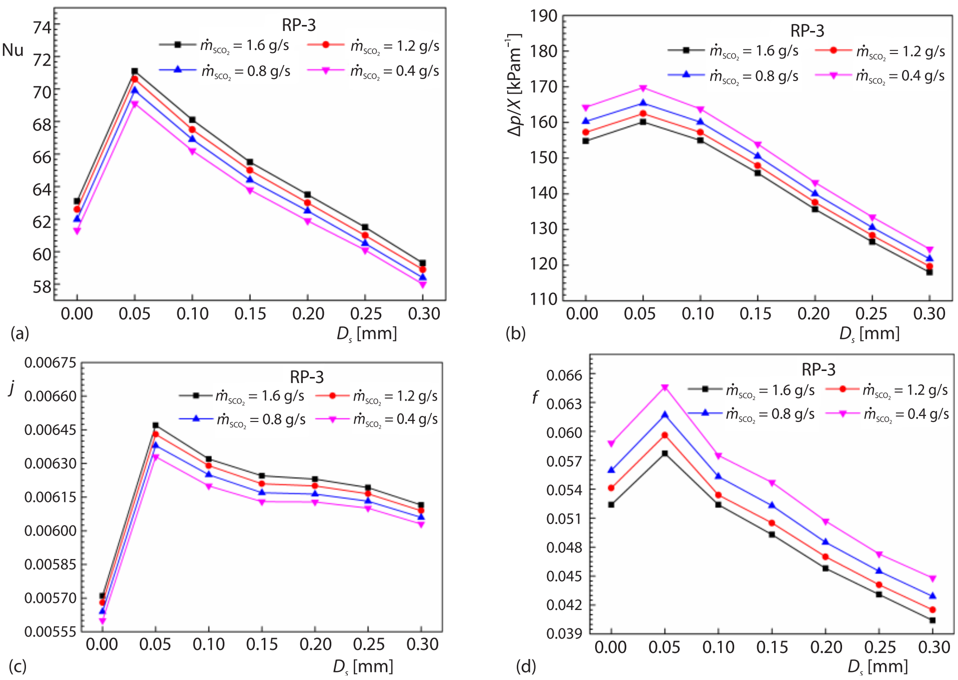

Figure 7. Overall performance of aviation kerosene at cold fluid channel with seven types of fins; (a) Nusselt number, (b) pressure drop per flow length, (c) Colburn *j* factor, and (d) Fanning friction factor

in the SCO_2 channel. This is because the viscosity of RP-3 in the cold channel decreases due to the improvement of the heat transfer performance, resulting in a smaller pressure loss in the channel. Figure 7(c) shows the trend of j for RP-3. Interestingly, the trend of j is also different from that of the SCO_2 channel. This is because the Reynolds number in the channel changes little due to the fixed mass-flow of aviation kerosene, and the trend of j is mainly affected by Nusselt number. Figure 7(d) shows the trend of f. It can be seen that the hydraulic performance in the kerosene channel first deteriorates and then improves.

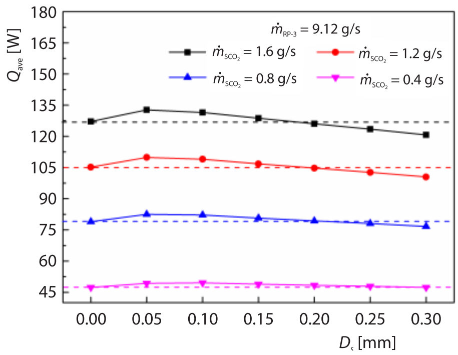

Figure 8. Heat transfer rate of seven types of fins under different working conditions

Figure 8 shows that the heat transfer rate of Fin2 is the largest among the seven airfoil fins. The heat transfer rates of Fin2, Fin3, and Fin4 are more significant than those of the original fins. The additional channels in the middle of the fins increase the heat transfer area, resulting in a more considerable heat transfer rate.

Figure 9 illustrates the effectiveness and NTU of the PCHE with different fins. It can be seen that ε and NTU first increase and then decrease with the increase of groove thickness, which indicates that the heat transfer performance of the PCHE first becomes better and then becomes worse with the increase of groove thickness. The Fin2 has the largest ε under various working conditions.

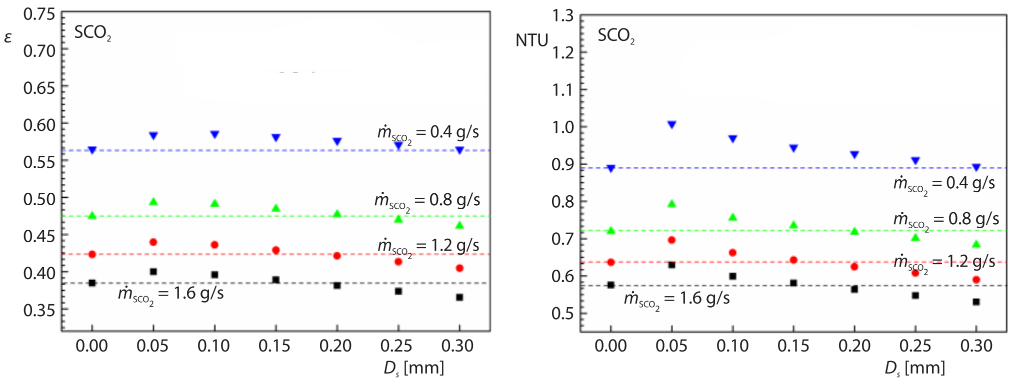

Figure 9. Effectiveness and number of heat transfer units of the PCHE

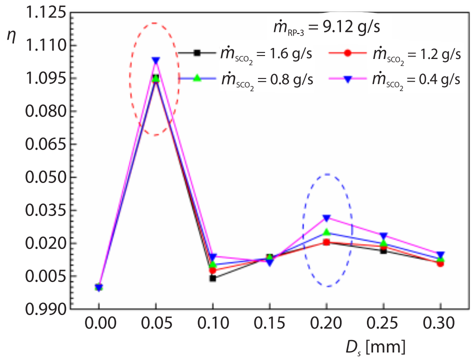

Figure 10. Enhanced ratio of different fins

Figure 10 presents the η of the seven fins under different working conditions. The overall performance of Fin2 and Fin5 is better than that of Fin1. As aforementioned, Fin2 has the best heat transfer performance but worse hydraulic performance. The thermal performance improvement is more significant than the decrease in hydraulic performance, resulting in a larger η.

When pursuing a higher heat transfer performance without considering the pressure drop, Fin2 is a better choice compared to the original airfoil fin. The thermal performance of Fin5 is the same as Fin1, but the hydraulic performance is much better. The η is larger than that of the original airfoil fin. The Fin5 is a better choice for pursuing a lower pressure drop without changing the heat transfer performance of the heat exchanger.

Thermal resistance matching

For a counterflow compact heat exchanger, the efficiency of the heat exchanger is reduced when the thermal resistance on one side is significantly lower or higher than that on the other side. The research of thermal resistance matching has an important influence on the design of the heat exchanger and the determination of the working conditions. Therefore, this subsection mainly focuses on the related issues of the heat resistance matching on both sides of the heat exchanger. For the flow and heat transfer in the channel, the main factors affecting the thermal resistance in the channel are the flow rate, heat transfer area, and properties of the fluid. In the aforementioned study, the comprehensive performance of Fin1, Fin2, and Fin5 is relatively good. Therefore, the thermal resistance of the three airfoil fins can be matched by adjusting the mass-flow rate of fuel when the mass-flow rate of supercritical carbon dioxide on the hot side is fixed. The optimal mass-flow ratio of SCO_2 to fuel under different working conditions is determined by calculating the thermal resistance on both sides.

As shown in fig. 11, the mass-flow of SCO_2 on the hot side is 0.0016 kg/s, 0.008 kg/s, and 0.016 kg/s, respectively, and the convective heat transfer coefficients on the hot and cold sides change with increasing fuel mass-flow. Since the size and arrangement of fins on both sides are the same, the matching of thermal resistance is transformed into the matching of convective heat transfer coefficients. When the convective heat transfer coefficients on both sides are equal, the thermal resistance is equivalent due to the same heat transfer area.

It can be seen from the figure that the flow ratio of fuel to SCO_2 increases gradually from 0.5-4. With the increase in fuel mass-flow, the convective heat transfer coefficient of the two channels increases gradually. As the mass-flow ratio of fuel to SCO_2 is 0.5, compared with the hot side channel, the convective heat transfer coefficient of the cold side channel is smaller, and the thermal resistance of the cold side channel is more considerable. According to eq. (14), the total heat transfer coefficient of the heat exchanger is controlled by convective heat transfer in the cold-side channel, when the wall thermal resistance is ignored. To improve the overall heat transfer coefficient of the heat exchanger, it is necessary to increase convective heat transfer in the cold side channel.

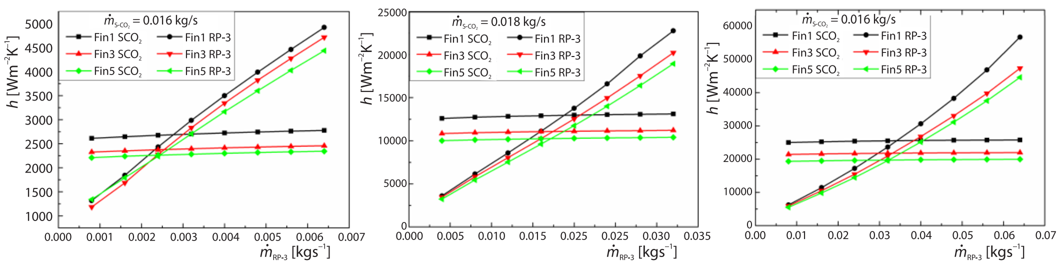

Figure 11. Thermal resistance matching under different working conditions; (a) $\dot m_{SCO_2}$= 0.0016kg/s, (b) $\dot m_{SCO_2}$=0.008kg/s, and (c) $\dot m_{SCO_2}$=0.016kg/s

Therefore, it has a significant influence on the design of the heat exchanger to determine the mass-flow on both sides under different working conditions. With the increase in groove thickness, the operating point with the same thermal resistance on both sides moves toward a lower fuel mass-flow rate. When the mass-flow rate of SCO_2 is 0.0016 kg/s, and the mass-flow rate of fuel is 0.024-0.03 kg/s, the thermal resistance on both sides is the same, and the ratio is approximately 1.5-2. When the mass-flow rate of CO_2 is 0.008 kg/s, and the mass-flow rate of fuel is 0.016-0.02 kg/s, the thermal resistance of both sides is equal, and the ratio is approximately 2-2.5.When the mass-flow rate of CO_2 is 0.016 kg/s, and the mass-flow rate of fuel is 0.032-0.04 kg/s, the thermal resistance of both sides is equal, and the ratio is approximately 2-2.5. Therefore, when the mass-flow ratio of fuel to supercritical SCO_2 is 1.5-2.5, the thermal resistance on both sides is the same.

Conclusion

The SCO_2 and China RP-3 aviation kerosene are used as working fluids to study the thermal-hydraulic performance of airfoil fin PCHE based on an SCO_2 cycle cooling system for scramjets. In this study, a novel structure of fins is proposed to improve the performance of PCHE, the effect of groove thickness on the flow and heat transfer performance of the PCHE is studied, and the enhancement mechanism of the novel fins is also discussed under various working conditions. The mass-flow ratio of fuel to SCO_2 is obtained by matching the thermal resistance under different working conditions, and the results show the following:

- A groove in the center of the airfoil fin is beneficial for improving the thermal-hydraulic performance of the airfoil fin PCHE. The streamline between the fins is not affected by the additional fluid channel in the middle of the fins, and the distribution of pressure and velocity in the fluid channel of the airfoil fin PCHE tends to be steady with increasing groove thickness.
- The groove in the center of the airfoil fin increases the heat transfer area. With increasing groove thickness, the thermal performance of the PCHE first improves and then deteriorates. Meanwhile, the groove in the center of the fins reduces the flow resistance in the fluid channel, and the overall hydraulic performance of the PCHE first worsens and then improves.
- Compared with the original airfoil fin, Fin2 improves the heat transfer performance, which is beneficial for improving the thermal efficiency of the SCO_2 cooling cycle. The Fin5 can reduce the pressure drop by up to 15% without affecting the thermal performance, which helps to reduce the pump loss.
- When the mass-flow rate in the channel is relatively low, to match the thermal resistance, the mass-flow ratio of fuel to SCO_2 is approximately 1.5-2. When the mass-flow rate in the passage is relatively high, the mass-flow ratio of fuel to SCO_2 is approximately 2-2.5.

Nomenclature

A – heat transfer area, [m^2]
C – heat capacity rate, [WK^{-1}]
C_p – specific heat capacity, [$Jkg^{-1}K^{-}1$]
D_h – hydraulic diameter, [m]
D_s – half the thickness of the groove, [m]
f – Fanning friction factor, [–]
j – Colburn j factor, [–]
h – convective heat transfer coefficient, [$Wm^{-2}K^{-1}$]
L – length of simulation model, [m]
$\dot{m}$ – mass-flow rate, [kgs^{-1}]
Δp – pressure drop, [Pa]
Q – heat transfer rate, [W]
y^+ – dimensionless wall distance, [–]

Greek symbols

ε – effectiveness of heat transfer, [–]
η – enhanced ratio, [–]
λ – heat conductivity, [Wm-1K-1]
μ – dynamic viscosity, [$kgm^{-}1s^{-1}$]
ρ – density, [kgm^{-3}]

Subscript

cold – cold side of PCHE
f – fluid
hot – hot side of PCHE
l – local
RES – representative surface
w – wall

References

[1] Naraghi, M., *et al*., Dual Regenerative Cooling Circuits for Liquid Rocket Engines, *Proceedings*, 42nd AIAA/ASME/SAE/ASEE Joint Propulsion Conference and Exhibit, Sacramento, Cal., USA, 2006
[2] Zhang, C., *et al*., Design and Heat Transfer Characteristics Analysis of Combined Active and Passive Thermal Protection System for Hydrogen Fueled Scramjet, *International Journal of Hydrogen Energy*, *40* (2015), 1, pp. 675-682
[3] Miao, H., *et al.*, Performance Analysis of Cooling System Based on Improved Supercritical CO_2 Brayton Cycle for Scramjet, *Applied Thermal Engineering*, *167* (2020), 114774
[4] Wickham, D. T., *et al*., Additives to Improve Fuel Heat Sink Capacity in Air/Fuel Heat Exchangers, *Journal of Propulsion and Power*, *24* (2008), 1, pp. 55-63
[5] Huang, H., *et al.*, Endothermic Heat-Sink of Jet Fuels for Scramjet Cooling, *Proceeding*s, 38th AIAA/ASME/SAE/ASEE Joint Propulsion Conference and Exhibit, Indianapolis, Ind., USA, 2002
[6] Balepin, V., Concept of the Third Fluid Cooled Liquid Rocket Engine, *Proceedings*, 42nd AIAA/ASME/SAE/ASEE Joint Propulsion Conference and Exhibit, Sacramento, Cal., USA, 2006
[7] Meshram, A., *et al*., Modelling and Analysis of a Printed Circuit Heat Exchanger for Supercritical CO_2 Power Cycle Applications, *Applied Thermal Engineering*, *109* (2016), Oct., pp. 861-870
[8] Lee, S.-M., Kim, K.-Y., Comparative Study on Performance of a Zigzag Printed Circuit Heat Exchanger with Various Channel Shapes and Configurations, *Heat and Mass Transfer*, *49* (2013), 7, pp. 1021-1028
[9] Kim, I. H., No, H. C., Physical Model Development and Optimal Design of PCHE for Intermediate Heat Exchangers in HTGR, *Nuclear Engineering and Design*, *243* (2012), Feb., pp. 243-250
[10] Lee, S.-M., Kim, K.-Y., A Parametric Study of the Thermal-Hydraulic Performance of a Zigzag Printed Circuit Heat Exchanger, *Heat Transfer Engineering*, *35* (2014), 13, pp. 1192-1200
[11] Ngo, T. L., *et al*., New Printed Circuit Heat Exchanger with S-Shaped Fins for hot Water Supplier, *Experimental Thermal and Fluid Science*, *30* (2006), 8, pp. 811-819
[12] Lin, Y. S., *et al*., Numerical Investigation on Thermal Performance and Flow Characteristics of Z and S Shape Printed Circuit Heat Exchanger Using S-CO2, *Thermal Science*, *23* (2019), Suppl. 3, pp. S757-S764
[13] Tsuzuki, N., *et al*., High Performance Printed Circuit Heat Exchanger, *Applied Thermal Engineering*, *27* (2007), 10, pp. 1702-1707
[14] Kim, D. E., *et al*., Numerical Investigation on Thermal-Hydraulic Performance of New Printed Circuit Heat Exchanger Model, *Nuclear Engineering and Design*, *238* (2008), 12, pp. 3269-3276
[15] Kwon, J. G., *et al*., Optimization of Air-Foil-Type PCHE for the Recuperator of Small Scale Brayton Cycle by Cost-Based Objective Function, *Nuclear Engineering and Design*, *298* (2016), Mar., pp. 192-200
[16] Kim, T. H., *et al*., Numerical Analysis of Air-Foil Shaped Fin Performance in Printed Circuit Heat Exchanger in a Supercritical Carbon Dioxide Power Cycle, *Nuclear Engineering and Design*, *288* (2015), July, pp. 110-118
[17] Xu, X., *et al*., Optimization of Fin Arrangement and Channel Configuration in an Air-Foil Fin PCHE for Supercritical CO_2 Cycle, *Applied Thermal Engineering*, *70* (2014), 1, pp. 867-875
[18] Ma, T., *et al.*, Effect of Fin-Endwall Fillet on Thermal Hydraulic Performance of Air-Foil Printed Circuit Heat Exchanger, *Applied Thermal Engineering*, *89* (2015), Oct., pp. 1087-1095
[19] Chu, W.-X., *et al.*, Study on Hydraulic and Thermal Performance of Printed Circuit Heat Transfer Surface with Distributed Air-Foil Fins, *Applied Thermal Engineering*, *114* (2017), Mar., pp. 1309-1318
[20] Cui, X., *et al.*, Numerical Study on Novel Air-Foil Fins for Printed Circuit Heat Exchanger Using Supercritical CO_2, *International Journal of Heat and Mass Transfer*, *121* (2018), June, pp. 354-366
[21] Ishizuka, T., *et al.*, Thermal-Hydraulic Characteristics of a Printed Circuit Heat Exchanger in a Supercritical CO_2 Loop, *Proceedings*, 11th International Topical Meeting on Nuclear Reactor Thermal-Hydraulics, Avignon, France, 2005, pp. 218-232

Paper submitted: April 8, 2022
Paper revised: June 17, 2022
Paper accepted: June 20, 2022